We are IntechOpen, the world's leading publisher of Open Access books Built by scientists, for scientists

6,900
Open access books available

186,000
International authors and editors

200M
Downloads

Our authors are among the

154
Countries delivered to

TOP 1%
most cited scientists

12.2%
Contributors from top 500 universities

WEB OF SCIENCE™

Selection of our books indexed in the Book Citation Index in Web of Science™ Core Collection (BKCI)

Interested in publishing with us?
Contact book.department@intechopen.com

Numbers displayed above are based on latest data collected.
For more information visit www.intechopen.com

Chapter 1

Cochlear Model for Hearing Loss

Miriam Furst

Additional information is available at the end of the chapter

http://dx.doi.org/10.5772/61189

Abstract

In many psychoacoustical tasks, hearing-impaired subjects display abnormal audiograms and poor understanding of speech compared to normal listeners. Existing models that explain the performance of the hearing impaired indicate that possible sources for cochlear hearing loss may be the dysfunction of the outer and inner hair cells. In this study, a model of the auditory system is introduced. It includes two stages: (1) a nonlinear time domain cochlear model with active outer hair cells that are driven by the tectorial membrane motion and (2) a synaptic model that generates the auditory nerve instantaneous rate as a response to the basilar membrane motion and is affected by the inner hair cell transduction efficiency. The model can fit both a normal auditory system and an abnormal auditory system with easily induced pathologies.

In typical psychoacoustical detection experiments, the ability of subjects to perceive a minimum difference in a physical property is measured. We use the model presented here to predict these performances by assuming that the brain behaves as an optimal processor that estimates a particular physical parameter. The performance of the optimal processor is derived by calculating its lower bound. Since neural activity is described as a nonhomogeneous Poisson process whose instantaneous rate was derived, the Cramer–Rao lower bound can be analytically obtained for both rate coding and all information coding.

We compared the model predictions of normal and abnormal cochleae to human thresholds of pure tones in quiet and in the presence of background noise.

Keywords: Cochlear model, outer hair cell, audiogram, hearing impairment, auditory nerve

1. Introduction

When sound waves enter the ear, they cause the basilar membrane (BM) that is located in the inner ear to vibrate. Since each place on the BM is tuned to a specific characteristic frequency

INTECH
open science | open minds

© 2015 The Author(s). Licensee InTech. This chapter is distributed under the terms of the Creative Commons Attribution License (http://creativecommons.org/licenses/by/3.0), which permits unrestricted use, distribution, and reproduction in any medium, provided the original work is properly cited.

(CF), the BM is able to separate the frequency components of sounds. The BM vibrations excite both the outer hair cells (OHC) and the inner hair cells (IHC). The OHCs act as local amplifiers, while the IHCs transduce the sound-induced vibrations into electrical impulses that propagate up the auditory cortex through the fiber tracks of the auditory pathway where the neural information is processed in a set of nuclei located in the auditory brainstem.

Damage can occur to the auditory system at any point along the auditory pathway. One of the most common impairments is OHC loss, frequently due to noise exposure. Often, when there is OHC loss , it is followed by IHC loss. Various diseases or old age can also injure different neurons along the auditory pathway.

Hearing impairment is characterized by abnormal audiograms and poor understanding of speech. The most frequent complaint is the inability to understand speech in a noisy environment. In many psychoacoustical tasks, hearing-impaired subjects yield lower thresholds than normal listeners (review by Moore [1]). For example, in monaural experiments, hearing-impaired subjects perform poorly in frequency discrimination tasks and in signal detection with a noisy background.

Models explaining the performance of hearing-impaired people [e.g., 2–9] indicate that the possible sources for cochlear hearing loss are the dysfunction of the outer hair cells and the loss of inner hair cells. The dysfunction of the OHCs reduces the gain of the active mechanism, which then tends to broaden the tuning curve and decrease the nonlinear effects. However, these models do not adequately predict hearing impairment performance [10, 11].

The purpose of this chapter is to introduce a comprehensive, nonlinear time domain cochlear model [6, 12–14], followed by a model of the auditory nerve (AN) response [7, 13, 16, 17] that can be used to predict hearing abilities of people with normal cochlea as well as with abnormal cochlea that suffers from either OHC loss and/or IHC loss.

Quantitative psychoacoustical measures that determine the human ability to detect the smallest difference in the physical property of a stimulus are usually implemented by forced-choice experiments. This difference is referred to as a "just-noticeable difference" (JND). Siebert [18] showed that if one assumes that the brain is behaving as an optimal processor, then psychoacoustical JND measurements can be predicted from auditory nerve instantaneous rates. In this chapter, we use this approach to compare the model predictions to human hearing thresholds, both normal and impaired, in both a quiet environment and in the presence of background noise.

2. The human ear model

The mammalian ear is composed of the outer ear, the middle ear, and the inner ear. The outer ear includes the pinna, the ear canal, and the ear drum. The middle ear is an air-filled cavity behind the ear drum, which includes three small ear bones, the ossicles. The inner ear includes a snail-shaped structure, the cochlea (see schematic description in Figure 1A).The sound is directed by the outer ear through the ear canal to the eardrum. When sound strikes the ear

drum, the movement is transferred through the three bones of the middle ear to a flexible tissue called the oval window, finally reaching the upper fluid-filled ducts of the cochlea (see Figure 1). The upper cochlear ducts are called scala vestibuli, and the bottom duct is referred to as scala tympani. The space between the top and bottom ducts is labeled as scala media.

The middle ear's task is to match the impedance of the sound pressure in the air to that of the fluid. Movement of the fluid inside the upper cochlear duct results in a pressure difference between the upper and lower ducts. This pressure difference in turn causes the basilar membrane (the membrane that separates the scala tympani and scala media) to move.

Two types of auditory receptor cells inhabit the scala media, the inner and outer hair cells. The defining feature of those cells is the hair bundle on top of each cell. The hair bundle comprises dozens to hundreds of streocilia, which are cylindrical actin-filled rods. The streocilia are immersed in endolymph, a fluid that is rich in potassium and characterized by an endocochlear potential of +80 mV. The streocilia move with the basilar membrane displacement. Their deflection opens mechanically gated ion channels that allow any small, positively charged ions (primarily potassium and calcium) to enter the cell. The influx of positive ions from the endolymph in the scala media depolarizes the cell, resulting in a receptor potential. The roles of the OHCs and IHCs on the function of the cochlea are very different. While the OHCs act as local amplifiers, the IHCs innervate the auditory nerve. The OHCs lay on the basilar membrane, and their upper part is embedded in a gel-like membrane, the tectorial membrane (TM). An increase in the OHC receptor potential causes a decrease in its length [19], which in turn enhances the BM movement. The hair bundles of the IHC move freely in the scala media. The change in their receptor potential opens voltage-gated calcium channels that release neurotransmitters at the basal end of the cell, which trigger action potentials in the attached nerve.

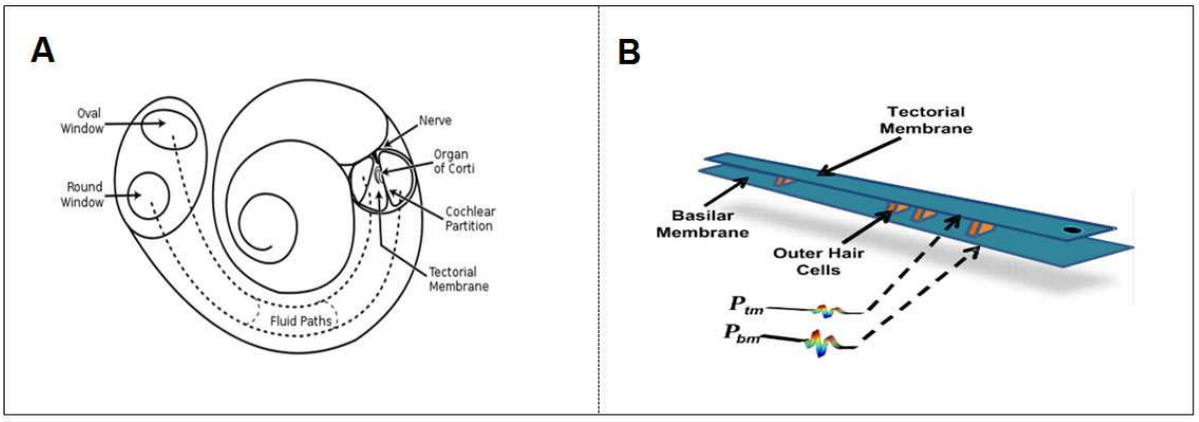

Figure 1. Schematic representation of the cochlea: (A) the snail-shaped structure of the cochlea; (B) schematic description of the Organ of Corti, emphasizing that the BM and the TM are attached by the OHCs.

Modeling the human ear requires a detailed model of the cochlea and the middle and outer ears. A common approach is to model the inner ear as a one-dimensional structure [e.g., 6, 14,

20–23] with the cochlea regarded as an uncoiled structure with two fluid-filled compartments with rigid walls that are separated by an elastic partition, the basilar membrane. The cochlear partition, whose mechanical properties are describable in terms of point-wise mass density, stiffness, and damping, is regarded as a flexible boundary between scala tympani and scala vestibuli. Thus, at every point along the cochlear duct, the pressure difference $P(x, t)$ across the partition drives the partition's velocity. By applying fundamental physical principles, such as the conservation of mass and the dynamics of deformable bodies, the differential equation for P is obtained by [e.g. 6]

$$\frac{\partial^2 P(x,t)}{\partial x^2} = \frac{2\rho\beta}{A}\frac{\partial^2 \xi_{\mathrm{bm}}(x,t)}{\partial t^2}, \tag{1}$$

where ξ_{bm} is the BM displacement, A represents the cross-sectional area of scala tympani and scala vestibuli, β is the BM width, and ρ is the density of the fluid in both the scala vestibuli and the scala tympani. The pressure on the BM (P_{bm}) is a result of both the difference in fluid pressure and the pressure caused by the OHCs (P_{ohc}). The relation between the pressures of BM, TM, and OHC is shown in Figure 1 [13], which can be interpreted as

$$\left.\begin{aligned} P_{\mathrm{bm}}(x,t) &= P(x,t) + P_{\mathrm{ohc}}(x,t) \\ 0 &= P_{\mathrm{ohc}}(x,t) + P_{\mathrm{tm}}(x,t) \end{aligned}\right\}. \tag{2}$$

The mechanical properties of both BM and TM are simulated as second-order oscillators that yield

$$\left.\begin{aligned} P_{\mathrm{bm}}(x,t) &= M_{\mathrm{bm}}(x)\cdot\frac{\partial^2 \xi_{\mathrm{bm}}}{\partial t^2}(x,t) + R_{\mathrm{bm}}(x)\cdot\frac{\partial \xi_{\mathrm{bm}}}{\partial t}(x,t) + K_{\mathrm{bm}}(x)\cdot\xi_{\mathrm{bm}}(x,t) \\ P_{\mathrm{tm}}(x,t) &= M_{\mathrm{tm}}(x)\cdot\frac{\partial^2 \xi_{\mathrm{tm}}}{\partial t^2}(x,t) + R_{\mathrm{tm}}(x)\cdot\frac{\partial \xi_{\mathrm{tm}}}{\partial t}(x,t) + K_{\mathrm{tm}}(x)\cdot\xi_{\mathrm{tm}}(x,t) \end{aligned}\right\}, \tag{3}$$

where K_{bm}, K_{tm}, R_{bm}, R_{tm}, M_{bm}, and M_{tm} are the effective stiffness, damping, and mass per unit area of BM and TM, respectively (see Table 1). The TM displacement is defined as ξ_{tm}.

Since the OHCs lie between the two membranes, their displacement is considered as

$$\xi_{\mathrm{ohc}} = \xi_{\mathrm{tm}} - \xi_{\mathrm{bm}}. \tag{4}$$

Each OHC is modeled by two sections, the apical and basal parts. The apical part is directed toward the endolymph of the gap between the TM and the reticular lamina (RL), while the basolateral part is embedded in the perilymph next to the supporting cells that are aligned

http://dx.doi.org/10.5772/61189

along the BM. When the OHCs' stereocilia move due to the relative displacement of the BM and the TM, the conductance of the apical part of the OHC is affected, which in turn causes a flow of potassium and calcium ions to the endolymph. Thus, a voltage drop is developed on the basal part of the OHC membrane [24].

An outer hair cell model is described by an equivalent electrical circuit in Figure 2 [6, 25]. The apical part is presented by its variable conductance ($G_a \approx \alpha \cdot \xi_{\text{ohc}}$) and its constant capacitance (C_a), while the basal part is presented by its constant conductance and capacitance, G_b and C_b, respectively. The electrical potential of the endolymph is $V_{\text{sm}}=80\,\text{mV}$, and the perilymph resting potential is $\psi_0=-70$ mV. Solving the equivalent electrical circuit by using Kirchhoff laws [6] yields the differential equation for ψ_{ohc}, the OHC's membrane voltage:

$$\frac{d\psi_{\text{ohc}}}{dt}+\omega_{\text{ohc}}\cdot\left(\psi-\psi_0\right)=\eta\cdot\xi_{\text{ohc}}, \tag{5}$$

where $\omega_{\text{ohc}}\approx G_b/C_b=1000\,\text{Hz}$, which represents the cutoff frequency of the OHC's membrane and $\eta=\alpha\cdot V_{\text{sm}}/\left(C_b+C_a\right)=\text{const.}$ (see Table 1).

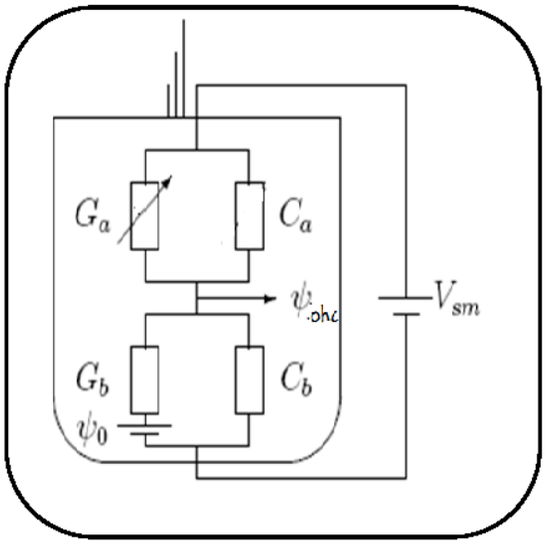

Figure 2. The equivalent electrical circuit of the outer hair cell.

An OHC's length changes due to the electrical potential developed on the OHC membrane and is defined as Δl_{ohc}. It is usually described as a sigmoid function [26–28]:

$$\Delta l_{\text{ohc}}=\alpha_s\frac{e^{\left(-2\cdot\alpha_l\cdot\psi\right)}-1}{e^{\left(-2\cdot\alpha_l\cdot\psi\right)}+1}=\alpha_s\tanh\left(-\alpha_l\cdot\psi\right), \tag{6}$$

where α_l and α_s are constants (see Table 1).

The pressure developed by each OHC (P_{ohc}) is obtained from the spring properties of the OHC [6]. Let's define $\gamma_{\text{ohc}}(x)$ as the OHC effective index. It represents the effective distribution of the OHCs along the cochlear partition. Therefore, the OHC pressure is obtained by

$$P_{\text{ohc}}(x,t) = \gamma_{\text{ohc}}(x) \cdot K_{\text{ohc}}(x) \cdot \left[\xi_{\text{ohc}}(x,t) - \Delta l_{\text{ohc}}(x,t) \right], \tag{7}$$

where K_{ohc} is the OHC's stiffness (Table 1). A cochlea with no active OHC is obtained by $\gamma_{\text{ohc}}(x)=0$, whereas $0.5 \le \gamma_{\text{ohc}}(x) \le 0.6$ yielded an optimal cochlea that best fits physiological data [13].

The ear model described by Eqs. (1)–(7) is solved by applying initial and boundary conditions. The boundary conditions are

$$\left.\begin{aligned} &\left.\frac{\partial P(x,t)}{\partial x}\right|_{x=0} = 2\rho C_{\text{ow}} \frac{\partial^2 \xi_{\text{ow}}(t)}{\partial t^2} \\ &P(L_{\text{co}},t) = 0 \end{aligned}\right\}, \tag{8}$$

where L_{co}=3.5 cm is the cochlear length, $\xi_{\text{ow}}$is the oval window displacement, and C_{ow} is the coupling factor of the oval window to the perilymph. In order to obtain ξ_{ow}, the middle ear model was applied [29] as expressed by the following differential equation:

$$\frac{d^2 \xi_{\text{ow}}(t)}{d^2 t} + \gamma_{\text{OW}} \cdot \frac{d\xi_{\text{ow}}(t)}{dt} + \omega_{\text{OW}}^2 \xi_{\text{OW}}(t) = \frac{1}{\sigma_{\text{OW}}} \left[P(o,t) + \Gamma_{\text{me}} P_{\text{in}}(t) \right], \tag{9}$$

where σ_{ow} is the oval window areal density, γ_{ow} is the oval window resistance, and ω_{ow} is the oval window resonance frequency. The mechanical gain of the ossicles is denoted by Γ_{me} (see Table 1). $P_{\text{in}}(t)$ is the input acoustic stimulus.

The initial conditions are

$$\left.\begin{aligned} &\xi_{\text{bm}}(x,0) = \left.\frac{\partial \xi_{\text{bm}}(x,t)}{\partial t}\right|_{t=0} = 0; \quad \xi_{\text{tm}}(x,0) = \left.\frac{\partial \xi_{\text{tm}}(x,t)}{\partial t}\right|_{t=0} = 0; \quad \xi_{\text{ow}}(0) = \left.\frac{\mathrm{d}\xi_{\text{ow}}(t)}{\mathrm{d}t}\right|_{t=0} = 0 \\ &\psi_{\text{ohc}}(x,0) = \psi_0 \end{aligned}\right\}. \tag{10}$$

Parameter	Value	Description
A	0.5	Cross-sectional area of the cochlea scalae $[cm^2]$
ρ	1	Perilymph density $[g/cm^3]$
β	0.003	Width of the basilar membrane [cm]
L_{co}	3.5	Cochlear length [cm]
K_{bm}	$1.282 \cdot 10^4 e^{-3x}$	Basilar membrane stiffness per unit area $[g/cm^2/s^2]$
R_{bm}	$0.25 \cdot e^{-0.6x}$	Basilar membrane damping per unit area $[g/cm^2/s]$
M_{bm}	$1.286 \cdot 10^{-6}$	Basilar membrane mass per unit area $[g/cm^2]$
K_{tm}	$3.97 \cdot 10^5 e^{-3x}$	Tectorial membrane stiffness per unit area $[g/cm^2/s^2]$
R_{tm}	$0.25 \cdot e^{-0.6x}$	Tectorial membrane damping per unit area $[g/cm^2/s]$
M_{tm}	0	Tectorial membrane mass per unit area $[g/cm^2]$
K_{ohc}	$400 \cdot e^{-3x}$	Outer hair cell membrane's stiffness $[g/s^2]$
α_s	10^{-6}	Peak to peak electromotility displacement [cm]
$1/\alpha_l$	$2 \cdot 10^{-6}$	Reference electromotility voltage [V]
ω_{ohc}	$2 \cdot \pi \cdot 1000$	Outer hair cell cutoff frequency [rad/s]
ψ_0	$-70 \cdot 10^{-3}$	Perilymph resting potential [V]
η	$3.14 \cdot 10^9$	[V/cm/s]
ω_{ow}	$2 \cdot \pi \cdot 1500$	Oval window cutoff frequency [Hz]
σ_{ow}	0.5	Oval window aerial density $[g/cm^2]$
γ_{ow}	$2 \cdot 10^4$	Oval window resistance $[1/s]$
C_{ow}	$6 \cdot 10^{-3}$	Coupling of oval window to perilymph [none]
Γ_{me}	21.4	Mechanical gain of ossicles [none]
η_{AC}	1	IHC AC coupling [V/s/cm]
η_{DC}	100	IHC DC coupling [V/cm]
Δ	$2 \cdot 10^{-3}$	IHC integration time [s]
A_{ihc}	1	AN coupling [spikes/s/V]
λ_{spont}^{H}	60	High spontaneous rate [spikes/s]
λ_{spont}^{M}	3	Medium spontaneous rate [spikes/s]
λ_{spont}^{L}	0.1	Low spontaneous rate [spikes/s]
λ_{sat}	500	Saturation rate [spikes/s]
A_H	70	Effective level threshold for high spontaneous rate [dB]
A_M	50	Effective level threshold for medium spontaneous rate [dB]
A_L	30	Effective level threshold for low spontaneous rate [dB]

Table 1. List of model parameters

2.1. Simulation results: The effect of outer hair cells loss

The above cochlear model was solved in the time domain by implementing a parallel algorithm on a commodity graphics processor unit (GPU) [14].The output of the model is the BM velocity ($\xi_{bm}(x, t)$) as a response to an acoustic stimulus $P_{in}(t)$.

Figure 3 represents the basilar membrane velocity relative to the input level at two points along the cochlear partition. The response was obtained by applying the model for a set of simple tones $P_0 \sin(2\pi ft)$ with a frequency of 100 Hz< f <8 kHz at different levels 0< P_0 ≤120 dB SPL. The gain plotted in Figure 3 was derived by $|\xi_{bm}(x)|/P_0$, where x =0.67 cm from the stapes (Figure 3A) and x =1.8 cm from the stapes (Figure 3B). Each solid line was obtained from a different level for a normal cochlea ($\gamma_{ohc}(x)$=0.5). The broken line represents an abnormal cochlea with 100% OHC loss, which was derived by the model by substituting $\gamma_{ohc}(x)$=0. For the normal cochlea, the maximum sensitivity at x =0.67 cm from the stapes (Figure 3A) was obtained when the stimulus was at 4 kHz and 0 dB SPL. The sensitivity is reduced with the increase in the input level, and the maximum sensitivity was shifted to a lower frequency (about 1 kHz). These results are in agreement with experimental results [30]. Figure 3B represents a characteristic frequency of 1 kHz that yielded wider responses as a function of frequency for all input levels. However, the gain of the damaged cochlea (broken line in Figure 3) was independent of the input level at both locations. When substituting $\gamma_{ohc}(x)$=0 in the cochlear model's equations, the nonlinear terms are zeroed and the model becomes linear.

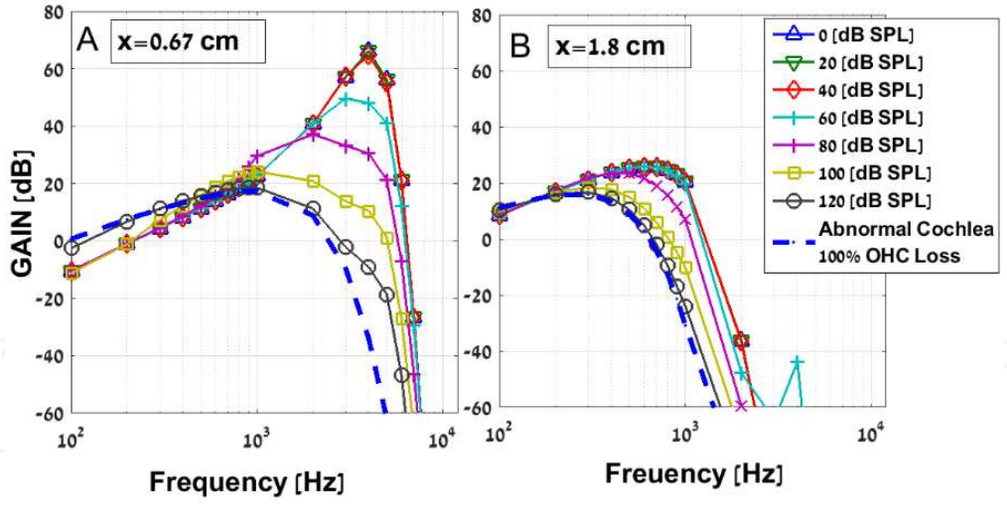

Figure 3. Derivation of the basilar membrane gain ($|\xi_{bm}(x_0)|/P_0$) as a function of input frequency at two locations along the cochlear partition: x = 0.67 cm from the stapes (A) and x = 1.8 cm from the stapes (B). Each solid line represents a different input level and a normal cochlea (γ_{ohc}=0.5). The broken line represents a damaged cochlea (γ_{ohc}=0). A similar gain was obtained for all input levels.

Figure 5 represents the relative BM velocity obtained by the model when the Hebrew word "SHEN" was introduced. The input word is presented in Figure 4 as a function of time (upper panel) and by its spectrogram (lower panel).

http://dx.doi.org/10.5772/61189

The absolute BM velocity in dB is presented in a color-coded two-dimensional image, whose x-axis represents the poststimulus time in milliseconds with its y-axis representing the distance from the stapes in cm. There are four images in Figure 5. The images in the left column represent a relative low input level (20 dB SPL), while the images in the right column represent an input level of 70 dB SPL. The upper panels represent a damaged cochlea with a 98% OHC loss (γ_{ohc}=0.01), while the lower panels represent a normal cochlea (γ_{ohc}=0.5). The difference between the normal and the damaged cochleae is clearly demonstrated in Figure 5 in both levels. In the damaged cochlea, the low-level stimulus yielded a BM vibration, which most likely will not be sufficient to evoke the neural response. Note that the maximum difference in the BM velocity between the normal and the damaged cochlea in response to the low-level stimuli is almost 40 dB. However, the maximum response between the two cochleae for the 70 dB input level is only 6 dB. This difference was induced by the nonlinear properties of the OHCs in the normal cochlea.

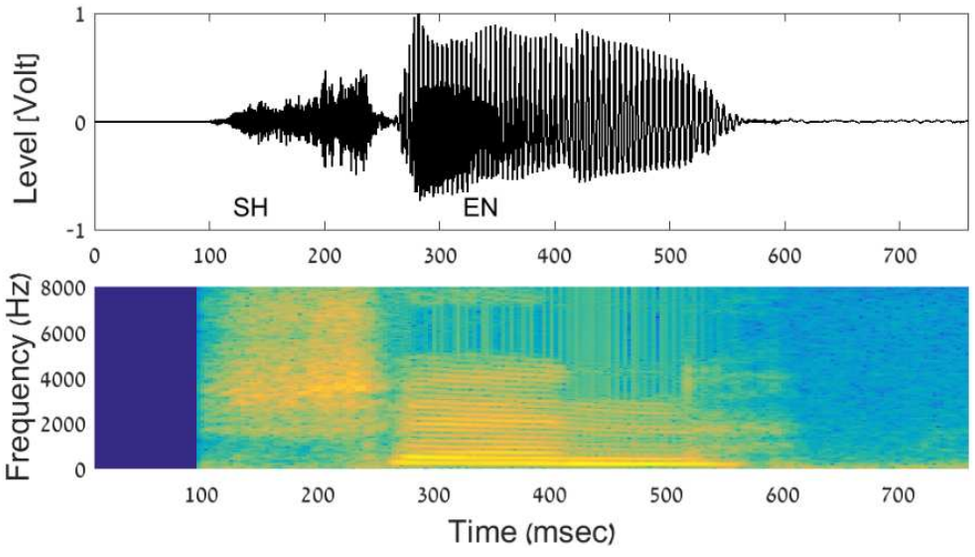

Figure 4. The Hebrew word "SHEN" pronounced by a female speaker. The sound pressure as a function of time (upper panel) and the correspondent spectrogram (lower panel).

The BM velocity in response to the consonant "sh" is very different in the four images in Figure 5. The maximum response was shifted toward the stapes when the amplitude was increased in the normal cochlea. In response to the high level stimuli, the maximum BM velocity obtained was closer to the stapes in the damaged cochlea than in the normal one.

3. Model of the Inner hair cell—auditory nerve synapse

The basilar membrane motion is transformed into neural spikes of the auditory nerve by the inner hair cells. The deflection of the hair-cell stereocilia opens mechanically gated ion channels that allow any small, positively charged ions (primarily potassium and calcium) to enter the cell [31]. Unlike many other electrically active cells, the hair cell itself does not fire an action

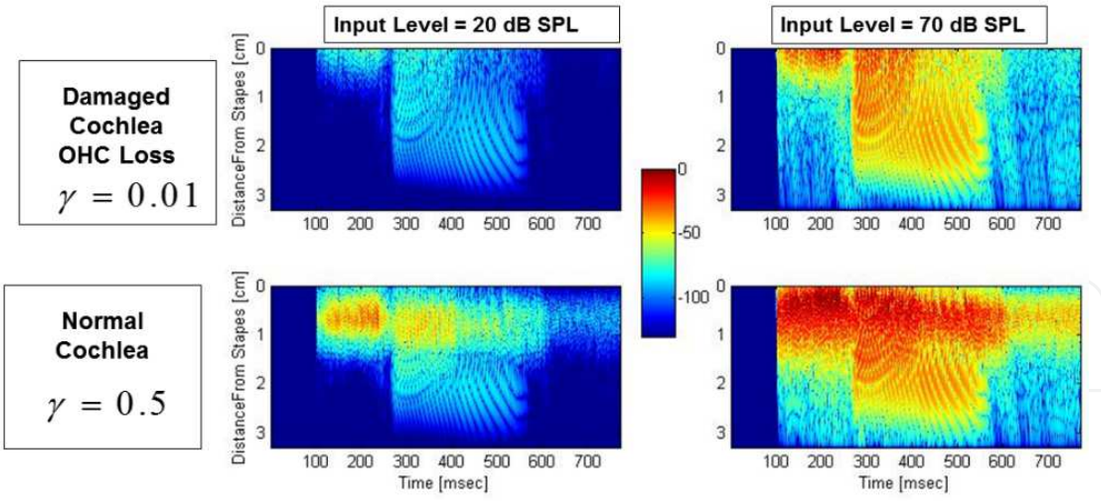

Figure 5. Relative BM velocity as a function of time along the cochlear partition as a response to the word "SHEN." The upper panels represent a damaged cochlea with outer hair cells loss and the lower panels represent a normal cochlea.

potential. Instead, the influx of positive ions from the endolymph in the scala media depolarizes the cell, resulting in a receptor potential. This receptor potential opens voltage-gated calcium channels; calcium ions then enter the cell and trigger the release of neurotransmitters at the basal end of the cell. The neurotransmitters diffuse across the narrow space between the hair cell and a nerve terminal, where they then bind to receptors and thus trigger action potentials in the nerve. In this way, the mechanical sound signal is converted into an electrical nerve signal. The IHCs chronically leak Ca^{+2}. This leakage causes a tonic release of neurotransmitter to the synapses. It is thought that this tonic release is what allows the hair cells to respond so quickly to mechanical stimuli. The quickness of the hair cell response may also be due to that fact that it can increase the amount of neurotransmitter release in response to a change as little as 100 μV in membrane potential.

Many models were developed for explaining the IHC's transduction abilities [16, 32, 33]. Some models focused on possible mechanisms for adaptation [17, 34–36]. Others were concerned with the biophysics of hair cells [37, 38] or the mechanoelectric transduction process [39].

One commonly simplified modeling approach to explain the IHC's role in the auditory system posits a nonlinear system that combines AC and DC responses followed by a random generator that creates spike trains [7, 16, 17, 40]. The model presented in this chapter is consistent with these principles.

The BM displacement stimulates the IHC cilia to move, its velocity ξ_{ihc} corresponding to the BM velocity (ξ_{bm}) by a nonlinear function, e.g.,

$$\dot{\xi}_{\text{ihc}} = \alpha_1 \tanh\left(\alpha_2 \cdot \dot{\xi}_{\text{bm}}\right) \approx \alpha_1 \cdot \left[\alpha_2 \cdot \dot{\xi}_{\text{bm}} - \frac{\left(\alpha_2 \cdot \dot{\xi}_{\text{bm}}\right)^3}{3} + \frac{2\left(\alpha_2 \cdot \dot{\xi}_{\text{bm}}\right)^5}{15} - \ldots\right]. \tag{11}$$

Since the BM displacement in this model is nonlinear as described by the mechanical model above, we ignore the nonlinear terms in Eq. (11) and assume that $\alpha_1 \cdot \alpha_2 = 1$; therefore, $\xi_{\mathrm{ihc}} \approx \xi_{\mathrm{bm}}$.

The mechanoelectrical receptors that are located in the IHC membrane yield an increase in the electrical potential (ψ_{ihc}) of the IHC membrane. A common modeling approach for the IHC's role in the auditory system is based on a nonlinear system that combines AC and DC responses [7, 40]. The DC level represents the firing responses without any synchrony to the input stimuli and the AC level represents the synchronized firing response (typical at low frequencies). The DC component includes a high-pass filter followed by a moving average filter of 2 ms long; the AC component consists of a low-pass filter. In order to account for physiological observations that demonstrated a reduction in synchronization as the frequency of the stimulus increases[41], we chose a low-pass filter with a cutoff frequency of 1000 Hz, with a slope of 30 dB/decade. In practice, ψ_{ihc} is obtained by

$$\psi_{\mathrm{ihc}}\left(x,t\right) = e^{\gamma_{\mathrm{ihc}}(x)} \cdot \left\{ \eta_{\mathrm{AC}} \cdot \dot{\xi}_{\mathrm{ihc}}\left(x,t\right) * h_{\mathrm{ihc}}\left(t\right) + \eta_{\mathrm{DC}} \cdot \int_{t-\Delta}^{t} \left\{ \dot{\xi}_{\mathrm{ihc}}\left(x,t\right) * \left[1 - h_{\mathrm{ihc}}\left(t\right)\right] \right\}^{2} dt \right\}, \tag{12}$$

where x represents the location of the IHC along the cochlear partition, $h_{\mathrm{ihc}}(t)$ is the impulse response of the low-pass filter that represents the IHC response, and η_{AC}, η_{DC}, and Δ are constants (see Table 1). The parameter $\gamma_{\mathrm{ihc}}(x)$ represents the IHC efficiency index. It was defined as a function of x, to allow variability in IHC efficiency along the cochlear partition. For normal cochlea, we chose $\gamma_{\mathrm{ihc}}(x)=8$, which was found to match experimental data. The efficiency of the IHC is reduced with a decrease of $\gamma_{\mathrm{ihc}}(x)$.

This IHC receptor potential opens voltage-gated calcium channels; calcium ions then enter the cell and trigger the release of neurotransmitters at the basal end of the cell. The neurotransmitters diffuse across the narrow space between the hair cell and a nerve terminal where they then bind to receptors and thus trigger action potentials in the nerve.

The neural activity in the auditory system is irregular since a specific neuron might respond with a single spike or several spikes to a given stimuli [42]. The origin of the stochastic activity of neurons is poorly understood. This activity results in both intrinsic noise sources that generate stochastic behavior on the level of the neuronal dynamics and extrinsic sources that arise from network effects and synaptic transmission [43]. Another source of noise that is specific to neurons arises from the finite number of ion channels in a neuronal membrane patch [31, 44].

There are a number of different ways that have emerged to describe the stochastic properties of neural activity. One possible approach relates to the train of spikes as a stochastic point process. For example, in their earlier studies, Alaoglu and Smith [45] and Rodieck et al. [46] suggested that the spontaneous activity of the cochlear nucleus can be described as a homogeneous Poisson process. Further investigations of the auditory system described the neural

response as a nonhomogeneous Poisson point process (NHPP) whose instantaneous rate depends on the input stimuli [47, 48].

In the present chapter, we relate to the neural activity as NHHP, and thus only the instantaneous rate (IR) should be extracted. In order to derive IR, we use the Weber–Fechner law, which describes the relationship between the magnitude of a physical stimulus and the intensity or strength that people feel. This kind of relationship can be described by a differential equation:

$$dP = K\frac{dS}{S}$$

where dP is the differential change in perception, dS is the differential increase in the stimulus, and S is the stimulus at the instant. Integrating the above equation reveals $P = k \cdot \ln S + C$. Let us define $\lambda_{\mathrm{AN}}(x, t)$ as the IR obtained by the auditory fiber attached to location x along the cochlear partition, and let us assume that it relates to the perception of the physical parameter. On the other hand, $\psi_{\mathrm{ihc}}(x, t)$, the IHC electrical potential corresponds to the stimulus. Therefore, by applying the Weber–Fechner law, we obtained the relationship $\lambda_{\mathrm{AN}}(x, t) = \ln(\psi_{\mathrm{ihc}}(x, t)) + C$. However, the AN's IR should satisfy the following conditions: $0 < \lambda_{\mathrm{spont}} \le \lambda_{\mathrm{AN}}(x, t) \le \lambda_{\mathrm{sat}}$, where λ_{spont} and λ_{sat} are the spontaneous and saturation rates of the AN, respectively. Therefore, $\lambda_{\mathrm{AN}}(x, t)$ is obtained by

$$\lambda_{\mathrm{AN}}(x,t) = \min\left\{\lambda_{\mathrm{sat}}, \max\left\{\lambda_{\mathrm{spont}}, A_{\mathrm{ihc}} \cdot \ln\left(1 + u(\psi_{\mathrm{ihc}}(x,t))\right)\right\}\right\}, \tag{13}$$

where u is the step function and A_{ihc} is a constant (see Table 1).

In general, the auditory nerve response is divided into three types of fibers according to their spontaneous rates: a high spontaneous rate (HSR) that usually codes low-level stimuli, a medium spontaneous rate (MSR), and a high spontaneous rate (LSR) that generally codes high level stimuli. In order to include all types of auditory nerves, we substitute in Eq. (13) the relevant constants $\left[\lambda_{\mathrm{spont}}^{(\mathrm{H})}, A_{\mathrm{H}}; \lambda_{\mathrm{spont}}^{(\mathrm{M})}, A_{\mathrm{M}}; \lambda_{\mathrm{spont}}^{(\mathrm{L})}, A_{\mathrm{L}}\right]$ for the HSR, MSR, and LSR that yield the instantaneous rates $\left[\lambda_{\mathrm{AN}}^{(\mathrm{H})}(x, t), \lambda_{\mathrm{AN}}^{(\mathrm{M})}(x, t), \lambda_{\mathrm{AN}}^{(\mathrm{L})}(x, t)\right]$, respectively. The different types of ANs are distributed uniformly along the cochlear partition, where the most frequent fibers are those with a low spontaneous rate (about 60%).

The IRs (spikes per second) for the LSR fibers, $\lambda_{\mathrm{AN}}^{(\mathrm{L})}(x, t)$, as a response to the Hebrew word "SHEN" are exhibited in Figure 6 by color-coded images as a function of time (x-axis) and along the cochlear partition (y-axis). The basilar membrane velocity as a response to this word was shown in Figure 5 for two different levels. In Figure 6, the response to the high level stimulus (70 dB SPL) is displayed. Four images are presented in Figure 6, each representing a different type of cochlea. Each cochlea is defined by the two indices, γ_{ohc} and γ_{ihc}, which

represent the efficiency of the OHC and IHC, respectively. In this example, both indices were constant along the cochlear partition. For normal cochlea, we chose γ_{ohc}=0.5 and γ_{ihc}=8 ; these values exhibit the best fit to experimental data [13].

The upper-left image in Figure 6 represents a normal cochlea (γ_{ohc}=0.5; γ_{ihc}=8). The upper-right image corresponds to a cochlea with intact OHC but with 25% IHC loss (γ_{ihc}=6). A clear reduction in the instantaneous rate is shown. The maximum instantaneous rate was reduced from 160 spikes/s in the normal cochlea to 100 in the damaged one. Moreover, in the damaged cochlea, about 25% more instances (time and location along the cochlear partition) reached the spontaneous rate 0.1 spikes/s relative to the normal cochlea.

The two lower images in Figure 6 represent cochleae with 98% OHC loss (γ_{ohc}=0.01). The BM response was changed as Figure 5 shows. Thus, the reduction in the instantaneous rate corresponds entirely to the decrease in BM velocity when the cochlea has intact IHCs (lower-left image). For a cochlea with both OHC and IHC loss (lower-right image), the instantaneous rate was reduced because of both losses. The response to the high frequencies that correspond to the syllable "SH" almost vanished.

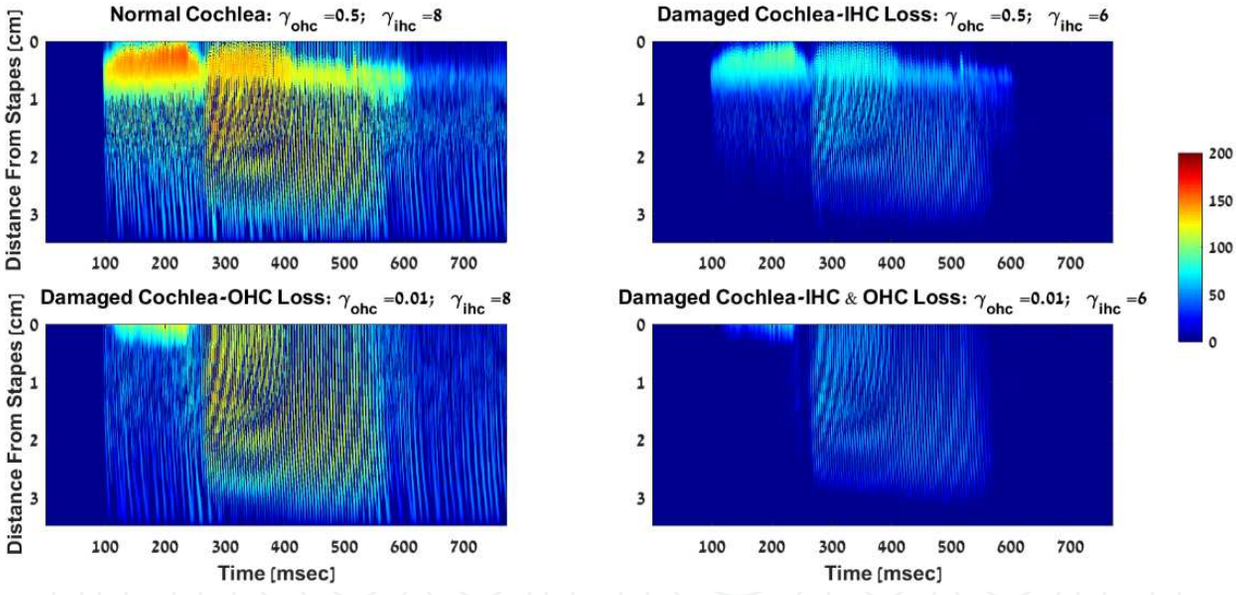

Figure 6. Derived instantaneous rates as a response to the Hebrew word "SHEN" at 70 dB SPL. Each panel represents a different type of ear. The upper-left panel represents a normal cochlea. The upper-right panel represents a cochlea with IHC loss. The lower-left panel represents a cochlea with OHC loss and the lower-right panel represents both IHC and OHC loss.

4. Threshold estimation based on the auditory nerve

The hearing threshold, defined as the lowest threshold of acoustic pressure sensation, is usually determined by quantitative psychoacoustical experiments in which the human ability

to detect the smallest difference in the stimulus' physical property is obtained. This difference is referred to as a just-noticeable difference (JND). In such experiments, a subject must distinguish between two close time (t) dependent stimuli: $s(t, \alpha)$ and $s(t, \alpha + \Delta\alpha)$, where α is a given physical property. The JND(α) will be the minimum $\Delta\alpha$ a person can perceive. The parameter α represents any physical property of the stimulus that can be measured such as frequency or level in monaural stimulus.

Comparing the behavioral JND and the neural activity is possible if one assumes that the neural system estimates the measured parameters. Siebert [18] obtained such a comparison when the JND of a single tone's frequency and level was compared to the neural activity of the auditory nerve. Siebert's findings were based on the assumption that the auditory nerve (AN) response behaves as an NHPP, and the brain acts as an unbiased optimal estimator of the physical parameters. Thus, the JND is equal to the standard deviation of the estimated parameter and can be derived by lower bounds such as the Cramer–Rao lower bound. Heinz et al. [49]) generalized Sibert's results to a larger range of frequencies and levels.

In a psychoacoustical JND experiment, the yielded JND value is obtained when $d' = 1$, which is expressed by:

$$d' = \frac{E\left[\hat{\alpha} \mid \alpha^*\right] - E\left[\hat{\alpha} \mid \left(\alpha^* + \Delta\alpha\right)\right]}{std\left(\hat{\alpha} \mid \alpha^*\right)} = \frac{\Delta\alpha}{std\left(\hat{\alpha} \mid \alpha^*\right)}, \tag{14}$$

where $E[\hat{\alpha} \mid \alpha^*] = \alpha^*$, α^* is the true value of α, and $\hat{\alpha}$ is the estimated value of α. Therefore, $d' = 1$, yields the relations $\Delta\alpha = std(\hat{\alpha} \mid \alpha^*)$, which implies

$$\mathrm{JND}\left(\alpha^*\right) = std\left(\hat{\alpha} \middle| \alpha^*\right). \tag{15}$$

When the estimation is based on neural activity that behaves as NHPP, there are two possible ways to analyze the performance. The first way is referred to as "rate coding" (RA), which means that the performance is analyzed on the basis of the number of spikes. The second way is referred as "all information coding" (AI), indicating that in addition to the number of spikes in the interval, the timing of the discharge spikes is considered as well.

Let us define $N(0, T)$ as the random variable that represents the number of spikes in the time interval $[0, T]$. For the RA coding, the probability density function (pdf) of getting n spikes in the time interval of length T is obtained by

$$P_{\mathrm{RA}}\left(N\left(0,T\right) = n\right) = \frac{1}{n!}\left[\int_0^T \lambda\left(t,\alpha\right)dt\right]^n \exp\left\{-\int_0^T \lambda\left(t,\alpha\right)dt\right\}, \tag{16}$$

where $\lambda(t, \alpha)$ is the instantaneous rate of the nerve fiber that depends on both the time t and the physical parameter α. Given the RA pdf (Eq. (16)), the resulting Cramer–Rao lower bound (CRLB) is obtained by [50]

$$\mathrm{CRLB}_{\mathrm{RA}}\left(\alpha^*\right)=\left\{\frac{T}{\bar{\lambda}\left(\alpha^*\right)}\left[\left.\frac{\partial\bar{\lambda}\left(\alpha\right)}{\partial\alpha}\right|_{\alpha=\alpha^*}\right]^2\right\}^{-\frac{1}{2}} \tag{17}$$

where $\bar{\lambda}(\alpha)=\frac{1}{T}\int_0^T\lambda(t, \alpha)dt$ is the average rate.

For the AI coding, the probability density function of getting n successive neural spikes at a set of time instances is $[t_1, t_2, \ldots, t_n]$, where $0\le t_1<t_2<\ldots<t_n\le T$ is obtained by

$$P_{\mathrm{AI}}\left(N\left(0,T=n\right);t_1,\ldots,t_n\right)=\frac{1}{n!}\prod_{k=1}^{n}\lambda\left(t_k,\alpha\right)\exp\left\{-\int_0^T\lambda\left(t,\alpha\right)dt\right\}. \tag{18}$$

The resulting CRLB was derived by Bar David [51], which yields

$$\mathrm{CRLB}_{\mathrm{AI}}\left(\alpha^*\right)=\left\{\int_0^T\frac{1}{\lambda\left(t,\alpha^*\right)}\left[\left.\frac{\partial\lambda\left(t,\alpha\right)}{\partial\alpha}\right|_{\alpha=\alpha^*}\right]^2dt\right\}^{-\frac{1}{2}}. \tag{19}$$

In every unbiased system, the following relations hold:

$$std\left(\left[\hat{\alpha}\middle|\alpha^*\right]\right)\ge\mathrm{CRLB}_{\mathrm{RATE}}\left(\alpha^*\right)\ge\mathrm{CRLB}_{\mathrm{AI}}\left(\alpha^*\right). \tag{20}$$

In an optimal unbiased system, the standard deviation of the estimator can achieve the lower bounds. Since $\mathrm{JND}(\alpha^*)=std(\hat{\alpha}\mid\alpha^*)$ (Eq. 15), $\mathrm{JND}(\alpha^*)$ can be estimated by calculating $\mathrm{CRLB}_{\mathrm{RA}}(\alpha^*)$ or $\mathrm{CRLB}_{\mathrm{AI}}(\alpha^*)$. Comparing the estimated thresholds to experimental results can resolve the question whether the brain estimates the auditory thresholds according to RA or AI coding.

In order to apply the above-mentioned method for determining the auditory threshold, we should consider the responses of all 30,000 AN fibers that innervate each ear. Since the AN fibers are statistically independent [2], the d' theorem can be applied, which yields

$$\left(d'\right)^2 = \sum_{m=1}^{M}\left(d_m'\right)^2, \tag{21}$$

where M is the number of nerve fibers and d_m' is the d' (Eq. 14) that was derived for the mth fiber. Moreover,

$$std\left(\hat{\alpha} \mid \alpha^*\right) = 1\Big/\sqrt{\sum_{m=1}^{M}\left\{std_m\left(\hat{\alpha} \mid \alpha^*\right)\right\}^{-2}}, \tag{22}$$

where $std_m(\hat{\alpha} \mid \alpha^*)$ is the standard deviation of the estimator obtained by the mth fiber. Since the threshold is obtained when $d'=1$, it implies that in an optimal system,

$$JND\left(\alpha^*\right) = 1\Big/\sqrt{\sum_{m=1}^{M}\left\{CRLB_m\left(\alpha^*\right)\right\}^{-2}}, \tag{23}$$

where $\mathrm{CRLB}_m(\alpha^*)$ is the CRLB of the mth fiber.

Let us define the number of fibers attached to each location along the cochlear partition as $M(x)$. Thus, $\sum_{x\in[o,L_{CO}]} M(x)=30,000$, where L_{CO} is the cochlear length. For every location, three IRs were derived $\lambda_{\mathrm{AN}}^{(\mathrm{H})}(x, t)$, $\lambda_{\mathrm{AN}}^{(\mathrm{M})}(x, t)$, $\lambda_{\mathrm{AN}}^{(\mathrm{L})}(x, t)$ (Eq. 13), which correspond to the HSR, MSR, and LSR fibers, respectively. They are distributed uniformly along the cochlear partition with corresponding weights $[w_{\mathrm{L}}, w_{\mathrm{M}}, w_{\mathrm{H}}]$ (see Table 1). Therefore,

$$\mathrm{JND}\left(\alpha^*\right) = \frac{1}{\sqrt{F_{\mathrm{L}} + F_{\mathrm{M}} + F_{\mathrm{H}}}}, \tag{24}$$

where

$$\left.\begin{aligned} F_{\mathrm{L}} &= \sum_{x\in[o,L_{CO}]}\sum_{m=1}^{w_L\cdot M(x)}\left\{\mathrm{CRLB}_m^{(\mathrm{L})}\left(\alpha^*\right)\right\}^{-2} \\ F_{\mathrm{M}} &= \sum_{x\in[o,L_{CO}]}\sum_{m=1}^{w_M\cdot M(x)}\left\{\mathrm{CRLB}_m^{(\mathrm{M})}\left(\alpha^*\right)\right\}^{-2} \\ F_{\mathrm{H}} &= \sum_{x\in[o,L_{CO}]}\sum_{m=1}^{w_H\cdot M(x)}\left\{\mathrm{CRLB}_m^{(\mathrm{H})}\left(\alpha^*\right)\right\}^{-2} \end{aligned}\right\}. \tag{25}$$

http://dx.doi.org/10.5772/61189

Replacing *CRLB* in Eq. (24) with the corresponding $\mathrm{CRLB}_{\mathrm{RA}}(\alpha^*)$ or $\mathrm{CRLB}_{\mathrm{AI}}(\alpha^*)$, $\mathrm{JND}(\alpha^*)$is estimated by either RATE or AI coding.

4.1. Simulation results: rate or all information?

In order to calculate both $\mathrm{CRLB}_{\mathrm{RATE}}(\alpha^*)$ and $\mathrm{CRLB}_{\mathrm{AI}}(\alpha^*)$, the derivative of the instantaneous rate should be derived. We have used the following approximation:

$$\partial\lambda(t,\alpha)/\partial\alpha\big|_{\alpha=\alpha^*} \approx \frac{\lambda(t,\alpha^*+\Delta\alpha)-\lambda(t,\alpha^*)}{\Delta\alpha}. \tag{26}$$

Therefore, in deriving $\mathrm{JND}(\alpha^*)$ for any stimulus $s(t,\alpha^*)$, the IRs for both stimuli $s(t,\alpha^*)$ and $s(t,\alpha^*+\Delta\alpha)$ should be calculated. Two types of thresholds will be presented for tones in quiet and in the presence of noise. The quiet threshold was derived by substituting $\alpha^*=0$ that yielded $\lambda(t,\alpha^*)=\lambda_{\mathrm{spont}}$. For the thresholds in the presence of noise, $s(t,\alpha^*)$ is equal to the noise, and $s(t,\alpha^*+\Delta\alpha)$ is equal to the noise +tone with a level of $\Delta\alpha$.

We have calculated the amplitude thresholds as a function of frequency while using both types of coding, RA and AI. The derived thresholds are shown in Figure 7 along with normal equal-loudness-level contour at threshold (ISO 226:2003) [52]. The rate coding successfully predicts the ISO 226 standard while the AI coding yielded performances that are better by a few decibels. This difference was not sufficient for deciding what type of coding is used by the brain in order to determine the absolute thresholds. Deriving the thresholds in the presence of noise revealed a more significant difference between the two types of coding.

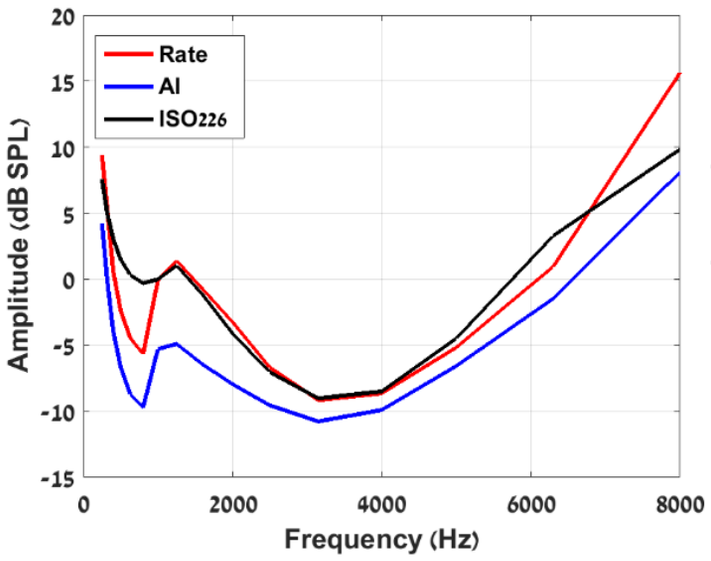

Figure 7. Estimated thresholds as a function of frequency obtained by a normal cochlea according to both rate and AI coding along with normal equal-loudness-level contour at threshold (ISO 226:2003).

In order to present the threshold of tones in the presence of noise, the smallest perceivable difference is presented in terms of difference limen (DL), which are defined as

$$\mathrm{DL} = 10 \cdot \log_{10}\left(1 + \frac{\Delta\alpha}{\alpha^*}\right), \tag{27}$$

where α^* corresponds to the noise level in Volts and $\Delta\alpha$ is the derived *JND* of the tone level in Volts. Figure 8 represents the DL of tones as a function of noise level for different frequencies. The noise was Gaussian white noise. The tone thresholds were derived by both types of coding (RA and AI), and they are presented in Figure 8 along with experimental data from Miller [54, 55]. Both types of coding succeeded in predicting the experimental result that the dependence of DL on noise level is independent of the tone's frequency. However, only RA coding yielded similar values of DL as a function of noise level. The AI coding revealed DL values that were lower by order of magnitude than the experimental result. This result convinced us that the brain is using rate coding in order to estimate tone amplitude.

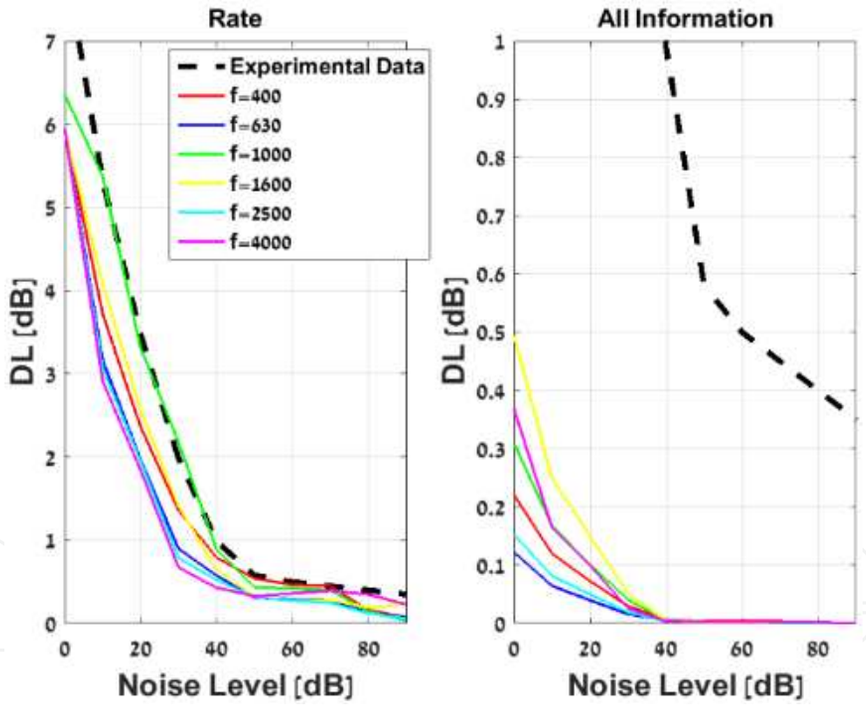

Figure 8. DL as a function of noise level as obtained by a normal cochlea according to both rate (left panel) and AI (right panel) coding. Each color represents a different frequency. The black broken line was replotted from [55].

4.2. Simulation results: Abnormal ears

Audiograms of the hearing impaired were estimated by subtracting the threshold of the damaged ear from the threshold defined by the equal loudness at threshold [52]. The estimated audiograms of different types of pathologies are shown in Figure 9. In all the estimated

http://dx.doi.org/10.5772/61189

audiograms, we assumed that both IHC and OHC loss were uniform along the cochlear partition, which implies that $\gamma_{ihc}(x)$=const. and $\gamma_{ohc}(x)$=const.

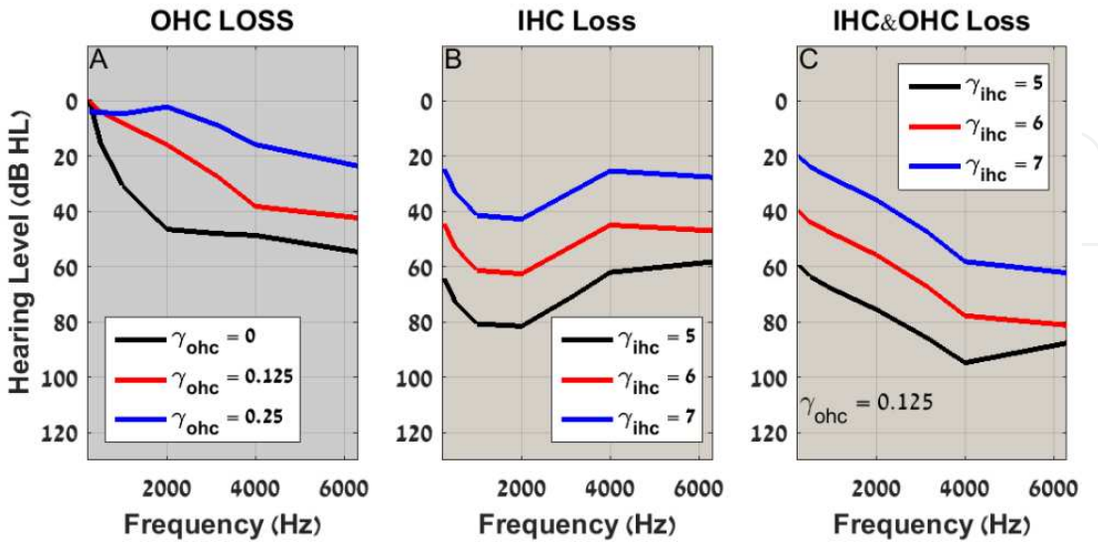

Figure 9. Estimated audiograms for different type of pathologies. Panel A represents cochleae with different degrees of OHC loss and intact IHC. Panel B represents cochleae with different degrees of IHC loss and intact OHC. Panel C represents cochlea with both IHC and OHC loss.

Three audiograms are exhibited in panel A of Figure 9. They were obtained with γ_{ihc}=8 (the normal value) and three values of γ_{ohc}=0, 0.125, 0.25 that represent 100%, 75%, and 50% of OHC loss, respectively. Due to OHC loss of 50%, no hearing loss was obtained up to 2 kHz. With 100% OHC loss, the estimated audiogram revealed a maximum hearing loss of about 60 dB at 6 kHz. Panel B of Figure 9 represents cochleae with no OHC loss (γ_{ohc}=0.5) but with different degrees of IHC loss, γ_{ihc}=5, 6, 7, which represents 37.5%, 25%, and 12.5% of IHC efficiency. Reduction in IHC efficiency caused a maximum hearing loss at 1000–2000 Hz. A combination of IHC and OHC loss is probably a more common pathology; an example of its effect is shown in Figure 9C. It represents cochleae with 75% OHC loss (γ_{ohc}=0.125) and different degrees of IHC loss. The maximum hearing loss was obtained at 4 kHz. The estimated audiogram with γ_{ihc}=7 resembles a typical mild audiogram while the one with γ_{ihc}=5 resembles a typical severe audiogram.

The effect of background noise on the threshold to tones is demonstrated in Figure 10, where DL is plotted as a function of noise level for different frequencies. As a result of OHC loss, γ_{ohc}=0, and a significant increase in DL was yielded especially at high frequencies relative to normal cochlea. The combination of IHC and OHC loss caused an increase in DL at all frequencies. It seems that the effect of IHC loss causes an increase in DL at low frequencies below 1000 Hz. This result might explain the difficulties of people with mild hearing loss to understand speech in a noisy background. The information of speech sounds is mainly included in the low frequency range.

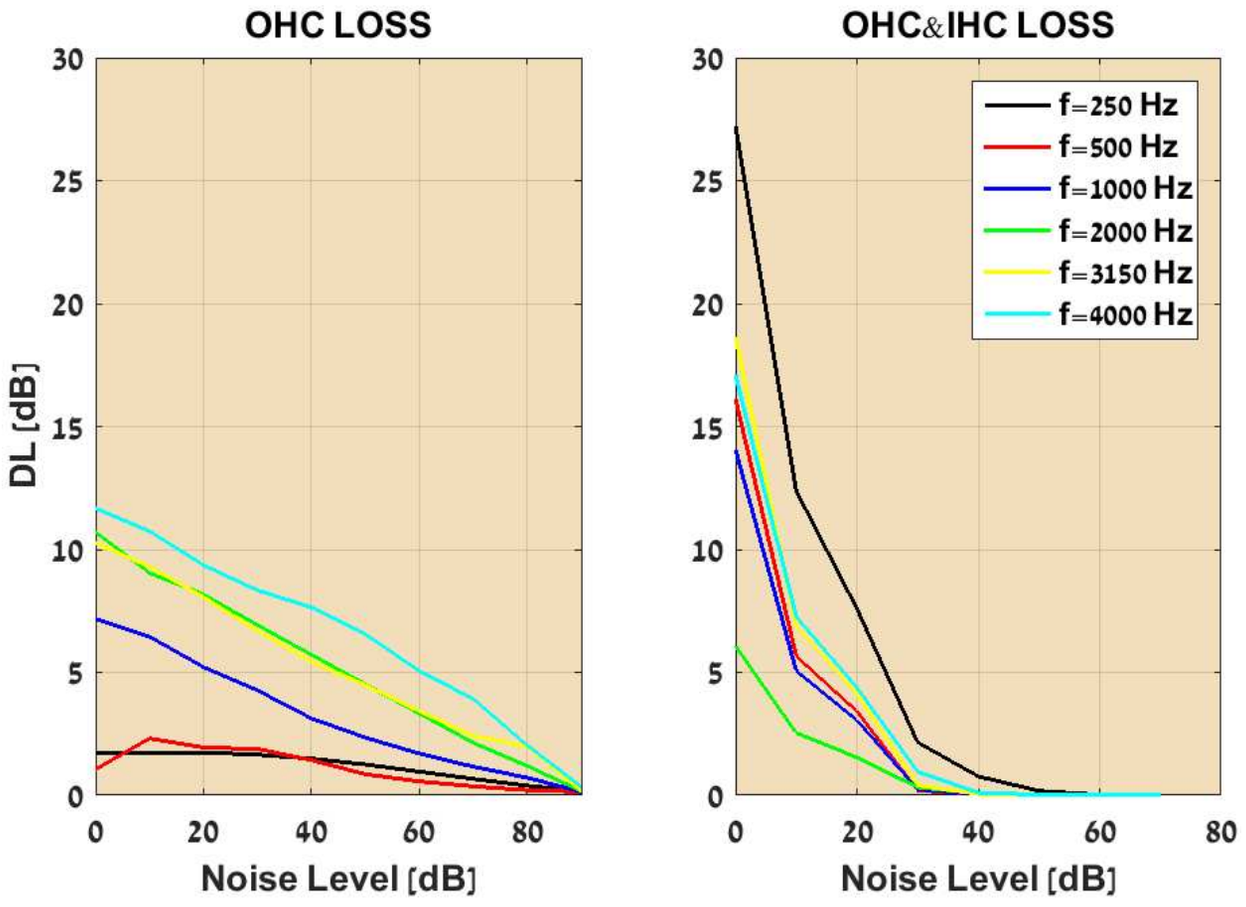

Figure 10. DL as a function of noise level as obtained by abnormal cochleae. Left panel represents a cochlea with 100% OHC loss ($\gamma_{ohc}=0$) and intact IHC. Right panel represents a cochlea with both IHC and OHC loss ($\gamma_{ohc}=0.125$; $\gamma_{ihc}=6$). Each color represents a different frequency.

5. Summary

In this study, a comprehensive model for the auditory system was introduced. It included a detailed, nonlinear time domain cochlear model with active outer hair cells that are driven by the tectorial membrane motion. Outer hair cell loss was indicated by an OHC efficiency index that could change along the cochlear partition. The second part of the model included a synaptic model that generates the auditory nerve's instantaneous rate as a response to basilar membrane motion and is affected by inner hair cell transduction efficiency. Since both inner and outer hair cell loss can be easily integrated in the model, the model is useful for demonstrating those pathologies.

In order to compare normal and abnormal human abilities to the model predictions, a comprehensive technique was introduced. It was based on the assumption that the brain behaves as an optimal processor and its task in JND experiments is to estimate physical parameters. The performance of the optimal processor can be derived by calculating its lower

bound. Since the neural activity was described as an NHPP, the Cramer–Rao lower bound was analytically derived for both rate and all information coding.

In this study, we have shown that the amplitude of tones in quiet and in the presence of background noise is most likely coded by the rate only. Pathological audiograms can be predicted by introducing reduced OHC and IHC efficiency indices. Moreover, the presence of noise causes a significant increase in DL. The effect of DL as a function of frequency depends on the type of hearing loss. In general, OHC loss mostly effects the high frequencies, while the effect of IHC loss is mostly expressed in the low frequencies.

The model presented in this paper can be used as a framework to explore different types of pathologies on the basis of audiograms obtained in quiet and in the presence of background noise.

Acknowledgements

This research was partially supported by the Israel Science Foundation grant no. 563/12. I want to express my great appreciation to my students who participated in this research over the years: Ram Krips, Azi Cohen, Vered Weiss, Noam Elbaum, Oren Cohen, Dan Mekrantz, Oded Barzely, Yaniv Halmut, and Tal Kalp.

Author details

Miriam Furst*

School of Electrical Engineering, Faculty of Engineering, Tel Aviv University, Tel Aviv, Israel

References

[1] Moore, B.C.J. (2007). Cochlear Hearing Loss. Wiley, West Sussex, United Kingdom.

[2] Heinz, M.G. (2010). Computational modeling of sensorineural hearing loss. In: Computational Models of the Auditory System, edited by R. Meddis, E.A. Lopez-Poveda, A.N. Popper, and R.R. Fay. Springer, New York, pp. 177–202.

[3] Jepsen, M.L., Ewert, S.D., and Dau, T. (2008). A computational model of human auditory signal processing and perception. J. Acoust. Soc. Am. 124, 422–438.

[4] Lopez-Poveda, E.A. and Meddis, R. (2001). A human nonlinear cochlear filterbank. J. Acoust. Soc. Am., 110, 3107–3118.

[5] Zilany, M.S.A., and Bruce, I.C. (2006). Modeling auditory-nerve responses for high sound pressure levels in the normal and impaired auditory periphery. J. Acoust. Soc. Am. 120: 1446–1466.

[6] Cohen A. and Furst M. (2004). Integration of outer hair cell activity in one-dimensional cochlear mode. J. Acoust. Soc. Am., 115:2185–2192.

[7] Carney L.H. (1993). A model for the responses of low-frequency auditory-nerve fibers in cat. J Acoust. Soc. Am. 93:401–417.

[8] Kates, J.M. (1991). A time-domain digital cochlear model. IEEE Trans. Signal Process. 39, 2573–2592.

[9] Goldstein, J.L. (1990). Modeling rapid waveform compression on the basilar membrane as multiple-bandpass-nonlinearity filtering. Hear. Res. 49, 39–60.

[10] Hopkins, K. and Moore, B.C.J (2011). The effects of age and cochlear hearing loss on temporal fine structure sensitivity, frequency selectivity, and speech reception in noise. J Acoust. Soc. Am. 130: 334–349.

[11] Jepsen, M.L. and Dau, T. (2011). Characterizing auditory processing and perception in individual listeners with sensorineural hearing loss. J. Acoust. Soc. Am., 129, 262–281.

[12] Furst, M. and Halmut, Y. (2006). Prediction for audiograms and otoacoustic emissions. In: Auditory Mechanisms: Processes and Models, edited by A.L. Nuttal, T. Ren, P. Gillespie, K. Grosh, and E. de Boer. World Scientific Publishing, pp. 384–385.

[13] Barzelay, O. and Furst, M. (2011). Time domain one-dimensional cochlear model with integrated tectorial membrane and outerhair cells. In: What Fire Is in Mine Ears Progress in Auditory Biomechanics, Vol 84, edited by C.A. Shera and E.S. Olson. American Institute of Physics, pp. 79–84.

[14] Sabo, D., Barzelay, O., Weiss, S., and Furst, M. (2014). Fast evaluation of a time-domain non-linear cochlear model on GPUs. J. Comput. Phys. 265: 97–113.

[15] Dau, T., Püschel, D., and Kohlrausch, A. (1996). A quantitative model of the effective signal processing in the auditory system. I. Model structure. J. Acoust. Soc. Am. 99, 3615–3622.

[16] Sumner, C., Lopez-Poveda, E., O'Mard, L., and Meddis, R.(2002). A revised model of the inner-hair cell and auditory-nerve complex. J. Acoust. Soc. Am. 111, 2178–2189.

[17] Zilany, M.S.A., Bruce, I.C., Nelson, P.C., and Carney, L.H. (2009). A phenomenological model of the synapse between the inner hair cell and auditory nerve: long-term adaptation with power-law. J. Acoust. Soc. Am. 126, 2390–2412.

[18] Siebert, W.M. (1970). Frequency discrimination in the auditory system: place or periodicity mechanism. Proc. IEEE 58, 723–730.

[19] Brownell, W.E., Bader, C.R., Bertrand D., and de Ribaupierre, I. (1985). Evoked mechanical responses of isolated cochlear outer hair cells. Science 227: 194–196.

[20] Zwislocki, J.J. (1950). Theory of the acoustical action of the cochlea. J. Acoust. Soc. Am. 22: 778–784.

[21] Zweig, G., Lipes, R., and Pierce, J.R. (1976). The cochlear compromise. J. Acoust. Soc. Am. 59: 975–982.

[22] Viergever, M.A. (1980). Mechanics of the inner ear a mathematical approach. Delft University of technology, Netherlands.

[23] Furst, M., Goldstein, J.L. (1982). A cochlear transmission line model compatible with psychophysics. J. Acoust. Soc. Am. 72: 717–726.

[24] Dallos, P.(2003). Organ of Corti Kinematics. J. Assoc. Res. Otolaryngol. 4: 416–421.

[25] Mountain, D.C. and Hubbard, A.E. (1995). Computational analysis of hair cell and auditory nerve processes. In: Auditory Computation, edited by H.L. Hawkins, T.A. McMullen, A.N. Popper, and R.R. Fay. Springer, pp. 121–156.

[26] Zheng, J., Madison, L.D., Oliver, D., Fakler, B., and Dallos, P. (2002). Prestin, the motor protein of outer hair cells. Audiol. Neurootol. 2002, 7: 9–12.

[27] He, D.Z.Z. and Dallos, P. (2000). Properties of voltage-dependent somatic stiffness of cochlear outer haircells. J. Assoc. Res. Otolaryngol. 1:64–81.

[28] Liu, Y.W. and Neely, S.T. (2009). Outer hair cell electromechanical properties in a nonlinear piezoelectric model. J. Acoust. Soc. Am. 126:751–761.

[29] Talmadge, C.L., Tubis, A., Long, G.L, and Piskorski, P. (1998). Modeling otoacoustic emission and hearing threshold fine structure. J. Acoust. Soc. Am. 104:1517–1543.

[30] Robles, L. and Ruggero, M.A. (2001). Mechanics of the mammalian cochlea. Physiol. Rev. 81:1305–1352.

[31] White, J.A., Rubinstein, J.T., and Kay, A.R. (2000). Channel noise in neurons. Trends Neurosci. 23: 131–137.

[32] Davis, H. (1965). A model for transducer action in the cochlea. Cold Spring Harb. Symp. Quant. Biol. 30, 181–189.

[33] Meddis, R., O'Mard, L.P., and Lopez-Poveda, E.A. (2001). A computational algorithm for computing nonlinear auditory frequency selectivity. J. Acoust. Soc. Am. 109: 2852–2861.

[34] Schroeder, M.R. and Hall, J.L. (1974). Model for mechanical to neural-transduction in the auditory receptor. J. Acoust. Soc. Am. 55: 1055–1060.

[35] Smith, R.L. and Brachman, M.L. (1982). Adaptation in auditory-nerve fibers: a revised model. Biol. Cybern. 44: 107–120.

[36] Meddis, R. (1986). Simulation of mechanical to neural transduction in the auditory receptor. J. Acoust. Soc. Am. 79: 702–711.

[37] Shamma, S.A., Chadwick, R.S., Wilbur, W.J., Morrish, K.A., and Rinzel,J.(1986). A biophysical model of the cochlear processing: intensity dependence of pure tone responses. J. Acoust. Soc. Am. 80: 133–145.

[38] Rattay, F., Gebeshuber, I.C., and Gitter, A.H. (1998). The mammalian auditory hair cell: a simple electric circuit model. J. Acoust. Soc. Am.103: 1558–1565.

[39] Corey, D.P., and Hudspeth, A.J. (1983). Kinetics of the receptor current in the bullfrog saccular hair-cells. J. Neurosci. 3: 962–976.

[40] Schoonhoven, R., Keijzer, J., Versnel, H., Prijs, V.F. (1993). A dual filter model describing single-fiber responses to clicks in the normal and noise-damaged cochlea. J. Acoust. Soc. Am. 95: 2104–2121.

[41] Palmer, A.M. and Russell, I.J. (1986). Phase-locking in the cochlear nerve of the guinea-pig and its relation to the receptor potential of inner hair-cells. Hear. Res. 24: 1–15.

[42] Kiang N.Y.S., Watanabe T., Thomas E.C., and Clark L.F. (1965). Discharge Patterns of Single Fibers in the Cat's Auditory Nerve. Cambridge MA, MIT press.

[43] Manwani, A. and Koch C. (1999). Detecting and estimating signals in noisy cable structures: I. neuronal noise sources. Neural Comput. 11: 1797–1829.

[44] Schneidman E., Freedman B., and Segev I. (1998). Channel stochasticity may be critical in determining the reliability and precision of spike timing. Neural Comput. 10: 1679–1703.

[45] Alaoglu, L. and Smith, N.M. Jr. (1938). Statistical theory of a scaling circuit. Phys. Rev. 53: 832 – 836.

[46] Rodieck, R.W., Kiang N.Y.-S., and Gerstein G.L. (1962). Some quantitative methods for the study of spontaneous activity of single neurons. Biophys. J. 2: 351–368.

[47] Gray, P.R. (1967). Conditional probability analyses of the spike activity of single neurons. Biophys. J. 10: 759–777.

[48] Rieke F., Warland D., van Steveninck R.D.R., and Bialek W. (1997). Spikes Exploring the Neural Code. MIT Press, Cambridge, Mass, USA.

[49] Heinz, M.G., Colburn, H.S., and Carney, L.H. (2001). Evaluating auditory performance limits: I. One-parameter discrimination using a computational model for the auditory nerve. Neural Comput. 13: 2273–2316.

[50] Snyder D.L. and Miller M.I. (1991). Random Point Processes in Time and Space. Springer-Verlag Berlin and Heidelberg GmbH & Co. K.

[51] Bar David, I. (1969). Communication under Poisson regime. IEEE Trans. Inf. Theory 15: 31–37.

[52] ISO226:2003:http://www.iso.org/iso/iso_catalogue/catalogue_tc/catalogue_detail.htm?csnumber=34222.

[53] Miller, G.A. (1947). Sensitivity to changes in the intensity of white noise and its relation to masking and loudness. J. Acoust. Soc. Am. 19: 609–619.

[54] Greenwood, D.D. (1993).The intensitive DL of tones: dependence of signal/masker ratio on tone level and on spectrum of added noise. Hear. Res. 65: 1–39.

IntechOpen

IntechOpen

IntechOpen

IntechOpen